Robotica (2019) volume 37, pp. 1020–1032. © Cambridge University Press 2019
doi:10.1017/S0263574718001418

Path Planning of Complex Pipe Joints Welding with Redundant Robotic Systems

H. Ghariblu* and M. Shahabi

Mechanical Engineering Department, University of Zanjan, Zanjan, Iran
E-mail: mehdi.shahabi@znu.ac.ir

(Accepted December 5, 2018. First published online: February 11, 2019)

SUMMARY
In this paper, a path planning algorithm for robotic systems with excess degrees of freedom (DOF) for welding of intersecting pipes is presented. At first step, the procedure of solving the inverse kinematics considering system kinematic redundancy is developed. The robotic system consists of a 6 DOF robotic manipulator installed on a railed base with linear motion. Simultaneously, the main pipe is able to rotate about its longitudinal axis. The system redundancy is employed to improve weld quality. Three different simulation studies are performed to show the effect of the robotic system kinematic redundancy to plan a better path for the welding of intersecting pipes. In the first case, it is assumed that robotic manipulator base and main pipe are fixed, and the path is planned only with manipulator joints motion. In the second case, only the robot base is free to move and the main pipe is fixed, and in the third case, the main pipe is free to rotate together with the base of the manipulator. It is seen that kinematic constraints according to the system's redundancy will help to plan the most efficient path for the welding of complex pipe joints.

KEYWORDS: Path planning; Intersecting pipes; Robotic; Welding; Redundancy.

1. Introduction

Robotic welding is a key component in order to accomplish a competitive and effective production. Successful implementation of robotic welding is especially seen throughout the automobile industry. However, other industries are still on the verge of utilizing robotic welding. Particularly, welding of intersecting pipes is widely used in several industries such as oil, gas, and petrochemicals, as well as in steam power plants, shipbuilding, etc. In these welding conditions, the exact design of the welding path is an important issue because of the complex geometry of the weld seam, especially when there are multi-welded parts located close together in a large workspace. In these cases, the welding torch must pass through the weld seam with specified velocity profile. Because weld seams in large pressure vessels and intersecting pipes have complex 3D curve, the quality of manual welding highly depends on the skill of the welder. On the other hand, automatic welding is able to guarantee the quality of welding along with increased productivity. Therefore, industrial owners are interested in robotic welding for the abovementioned applications instead of manual welding. For simple weld paths such as flat surface and straight line welding, employing a robot with 5 degrees of freedom (DOF) is usually sufficient. But in cases where obstacles are present in the workspace or if weld paths have a complex geometry, more DOF will be needed for welding. Because of the importance of these applications, in this paper an algorithm is proposed for path planning of interesting pipes using a redundant 6 DOF industrial robotic manipulator installed on a mobile linear railed base having the main pipe rotational positioner. The same path planning algorithm can be easily adapted for any other kinds of kinematic redundant robotic structures, such as gantry robots, mobile manipulators, or other kinds of complex welding geometries.

* Corresponding author. E-mail: ghariblu@znu.ac.ir

When the robotic manipulator has redundancy, researchers use this redundancy to reach some desired goals, for example, reduction of energy consumption,[1] overcoming discontinuity problem,[2] improving kinematic and dynamic performance,[3] motion planning considering obstacle avoidance,[4,5] etc. There are different techniques for redundancy resolution of robotic manipulators that are divided into three main categories, namely Jacobian-based methods,[6,7] null space methods,[8] and task augmentation methods.[9] Here we use a combination of Jacobian-based and task augmentation methods for redundancy resolution. A review of past work shows that the welding of these pipes has been less studied using 6 DOF industrial robots. Lu et al.[10] have controlled automated welding on a saddle curve. Chen et al.[11] have proposed a method for weld seam path planning of nozzles installed on a spherical head of pressure vessels that was an intersection curve of pipe to sphere. They have used a special welding machine installed on the branch pipe. Pose planning for the end-effector of the robot in the welding of intersecting pipes was presented by Liu et al.[12] They have extracted a mathematical model of the pipe intersection curve by considering two different conditions for weld seam coordinates. They have also used a special welding machine. Wu et al.[13] have considered the problem of coordinating multiple motion devices for welding with a focus on the problem of coordinating a three-axis positioning table and a six-axis manipulator. Their approach to the coordination problem was based on a subdivision of tasks. Ren et al.[14] have modeled weld seam and welding torch pose in the welding of intersected T-shaped pipes. Yao et al.[15] have developed a mechanism for pipe welding that had four revolute joints and one prismatic joint along main pipe axis. Tian and Lü[16] have proposed a tree-axis interpolation algorithm, similar to that used in CNC machines, to control the path in automated welding of tubular joints.

Some researchers have used 6 DOF commercial robots for path planning. Doan and Lin have introduced optimal robot placement with a consideration of redundancy problem for wrist-partitioned 6R articulated robots.[17] Some others have limited their research to path planning in the operating space. They did not study path planning benefiting from redundancy. Shi et al.[18,19] have proposed an industrial robotic algorithm for welding intersecting pipes, which considered the welding requirement in path planning, but not path planning limitation in joint space. Li et al.[20] have used Solidworks API CAD software for path planning. First, intersecting pipes were modeled in Solidworks, then a 3D intersection curve was specified by using several nodes on the curve. Then, a weld seam coordinate was assigned to each node. This program output was transferred to offline programming for commercial robots. Because of joint space limitation, there was no guarantee that the robot could travel the curve. Some other researchers have been exploring path planning of welding robot in the joint space using some intrinsic properties of welding such as functional redundancy due to unimportant rotation of the welding torch around its axis. Huo and Baron[21] have presented an algorithm to automatically adjust the parameters of singularity avoidance optimization and joint limit avoidance optimization. Leger and Angeles6 have proposed an algorithm for solving functional redundancy of 6 DOF commercial robots in applications such as welding that needs 5 DOF operational space.

Although all the aforementioned algorithms introduced redundancy resolution techniques for robotic welding of intersecting pipes, none of them simultaneously considered robot base motion, main pipe rotation, and manipulator excess DOF as redundant variables. As investigated in this paper, the combination of these extra DOFs enables us to make a possible path planning for complex pipe joint welding conditions. In this work, we propose an algorithm for path planning of a robotic welding system with redundancy in its motion. The redundancy of the system avoids joint limits and manipulator singularity in welding path planning. The flat welding condition for better controlling of welding pool and improving weld quality were other criteria to use system redundancy. The rest of the paper is organized as follows. Section 2 formulates the problem of inverse kinematics considering system redundancy that is more than 5 DOF operational space needed for robotic welding. In section 3, the trajectory planning algorithm for robotic welding of intersecting pipes is presented. In section 4, simulation studies of employing our algorithm considering different redundancy situations are presented. Finally, conclusions are drawn in Section 5.

2. Robotic Kinematics

Figure 1 shows an overview of the robotic manipulator's standard coordinate frames. In path 1, the welding torch pose is determined relative to the Ref. frame. This chain includes the Torch frame, Seam frame, Main frame, Station frame, and Ref frame. In path 2 the welding torch pose

https://doi.org/10.1017/S0263574718001418 Published online by Cambridge University Press

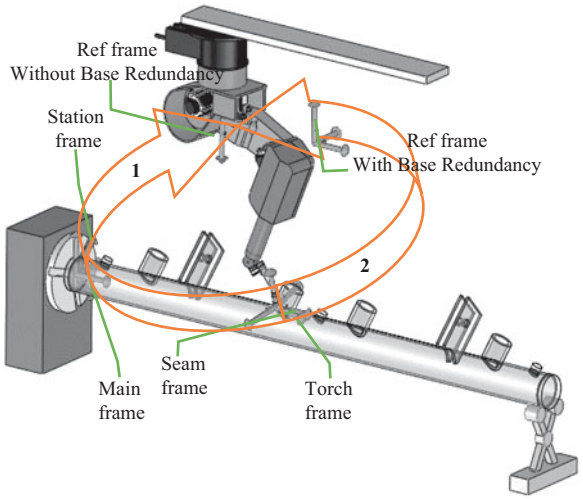

Fig. 1. Frames describing the robot motion.

is determined using inverse kinematic solution. This path includes the Torch frame, robotic arms' joints reference frames, and Ref frame. After determining path 1 homogenous transformation (HT), in path 2, joint variables are determined using inverse kinematics.

According to Fig. 1, path 1 HT is composed of:

$$ {}^{Ref}_{Torch}T = {}^{Ref}_{Station}T\,{}^{Station}_{Main}T\,{}^{Main}_{Seam}T\,{}^{Seam}_{Torch}T \tag{1} $$

where ${}^{Ref}_{Station}T$ is HT from the Station frame, which is fixed in the main pipe rotating stand, to the Ref frame. The location of Ref frame depends on robot base redundancy. Figure 1 shows the location of Ref frame with/without considering robot base redundancy. If redundancy is considered, Z_{Ref} is parallel to the longitudinal rails of the robot base, whereas if redundancy is not considered, Z_{Ref} is directed to the first revolute joint axis of the robot. ${}^{Ref}_{Station}T$ transformation is calculated as:

$$ {}^{Ref}_{Station}T = \begin{bmatrix} c\theta_{ref} & -s\theta_{ref}\,c\alpha_{ref} & s\theta_{ref}\,s\alpha_{ref} & a_{ref}\,c\theta_{ref} \\ s\theta_{ref} & c\theta_{ref}\,c\alpha_{ref} & -c\theta_{ref}\,s\alpha_{ref} & a_{ref}\,s\theta_{ref} \\ 0 & s\alpha_{ref} & c\alpha_{ref} & d_{ref} \\ 0 & 0 & 0 & 1 \end{bmatrix} \tag{2} $$

where $a_{ref}, d_{ref}, \alpha_{ref}, \theta_{ref}$ are calculated using homogeneous transformation rules.[22]

${}^{Station}_{Main}T$ is the HT from the Main frame to the Station frame. Figure 2 shows that the origin of two frames is coincident and their Y-axis is collinear. If workpiece positioner is not rotated, these two frames are coincident and ${}^{Station}_{Main}T$ is identity matrix; otherwise the Main frame is rotated relative to the Station frame by β angle:

$$ {}^{Station}_{main}T = \begin{bmatrix} cos\beta & 0 & sin\beta & 0 \\ 0 & 1 & 0 & 0 \\ -sin\beta & 0 & cos\beta & 0 \\ 0 & 0 & 0 & 1 \end{bmatrix} \tag{3} $$

${}^{Main}_{Seam}T$ is the HT from the Seam frame to the Main frame. Referring to Fig. 3, the pipe intersection curve can be described as $g(\theta)$ so that each point on the curve is exclusively determined by an angle θ around the branch pipe axis, as:

$$ \begin{cases} x_{brch} = r\ sin\,\theta \\ y_{brch} = csc\,\alpha\,\sqrt{R^2 - (r\ sin\,\theta + e)^2} - r\,\cot\alpha\,\cos\theta \\ z_{brch} = r\,\cos\theta \end{cases} \tag{4} $$

https://doi.org/10.1017/S0263574718001418 Published online by Cambridge University Press

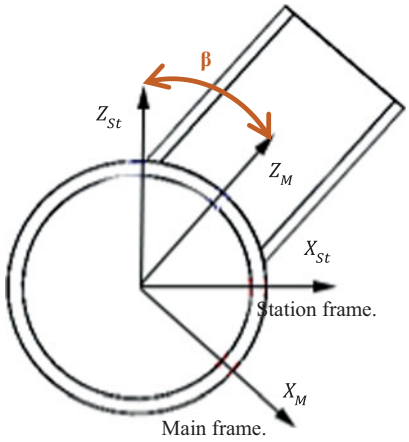

Fig. 2. The Main frame relative to the Station frame.

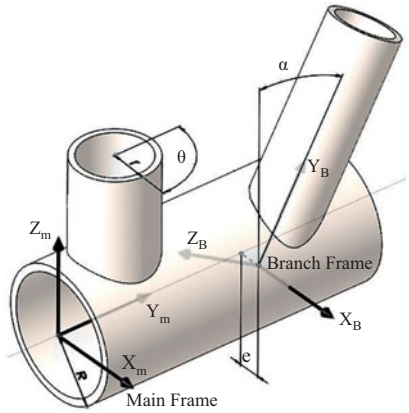

Fig. 3. The Branch frame relative to the Main frame.

The HT from the Branch frame to the Main frame is extracted from Fig. 3:

$$ {}^{Main}_{Branch}T = \begin{bmatrix} 1 & 0 & 0 & e \\ 0 & \cos\alpha & -\sin\alpha & 0 \\ 0 & \sin\alpha & \cos\alpha & 0 \\ 0 & 0 & 0 & 1 \end{bmatrix} \tag{5} $$

As Fig. 4 shows, the origin of Seam frame is located on the pipe intersection curve, where X-axis is directed along weld seam, and Z-axis coincides with the weld perpendicular bisector that bisects the dihedral angle between branch pipe tangent plane and main pipe tangent plane. The Y-axis is determined by the right hand rule.

Finally, the pipe intersection curve is determined using the HT from the Branch frame to the Main frame as well as the HT from the Seam frame to the Main frame as follows:

$$ {}^{Main}_{Seam}T = \begin{bmatrix} & & & x_{brch} + e \\ \{n\} & \{o\} & \{a\} & \cos\alpha\, y_{brch} - \sin\alpha\, z_{brch} \\ & & & \sin\alpha\, y_{brch} + \cos\alpha\, z_{brch} \\ 0 & 0 & 0 & 1 \end{bmatrix}, \begin{cases} n = \dfrac{n_m \times n_b}{|n_m \times n_b|} \\ o = \dfrac{n_m - n_b}{|n_m - n_b|} \\ a = \dfrac{n_m + n_b}{|n_m + n_b|} \end{cases} \tag{6} $$

https://doi.org/10.1017/S0263574718001418 Published online by Cambridge University Press

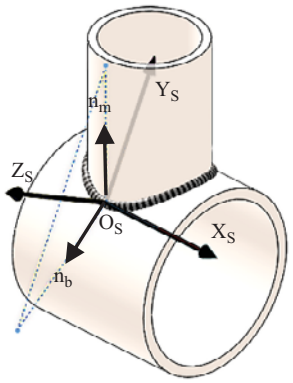

Fig. 4. Seam frame.

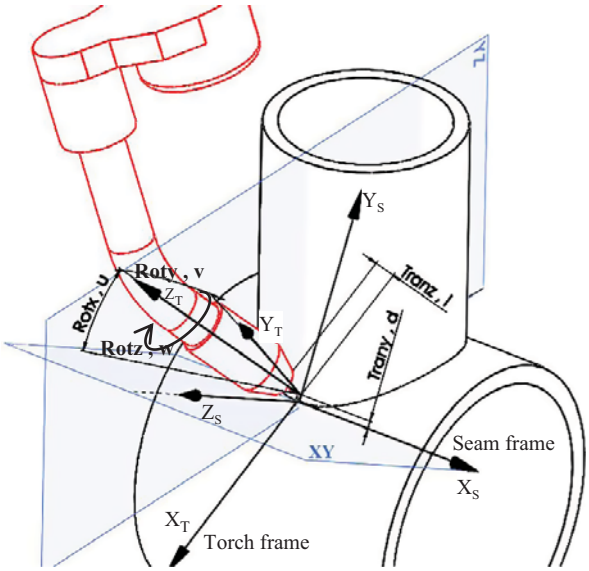

Fig. 5. Torch frame to Seam frame.

where n_m and n_b are, respectively, normal to the Main and Branch pipes that are located on the weld seam Os:[12]

$$\begin{cases} n_m = \left[\dfrac{r\sin\theta + e}{R} \quad 0 \quad \dfrac{\sqrt{R^2 - (r\sin\theta + e)^2}}{R} \right] \\ n_b = \left[\sin\theta \quad -\sin\alpha\cos\theta \quad \cos\alpha\cos\theta \right] \end{cases} \tag{7}$$

${}^{Seam}_{Torch}T$ is the HT from the Torch frame to the Seam frame. The Torch frame is the last frame that is assigned to the robot arms according to DH convention. Its origin is located at the tip of welding electrode, while its Z-axis coincides with welding electrode direction. Referring to Fig. 5 to describe this transformation, it is necessary to combine two transforms and three rotations that were used to define the welding specifications, including motion angle, work angle, torch redundancy angle, electrode extension, and torch weaving motion.

To describe electrode orientation during the welding process, two angles are defined. One is work angle, u, which is the angle between the Z-axis Seam and the projection of Z-axis Torch on YZ–Seam plane. When $u = 0$, the weld electrode coincides with the bisector of normal of the main and branch pipes. The other is motion angle, v, which is defined as the angle between the Z-axis Torch and YZ–Seam plane. When $v = 0$, the weld electrode is perpendicular to the weld seam.

https://doi.org/10.1017/S0263574718001418 Published online by Cambridge University Press

Electrode extension L is a parameter that is used to control weld deposition rate and depends usually on materials, welding transfer mode, application, etc. Another feature of the welding process is weaving motion, which increases the efficiency of welding via making the weld bead wider and preventing some weld defects such as lack of penetration at weld sides.

The weaving motion is perpendicular to the weld seam, and δ is half of its amplitude. Previously, to make a weaving motion, an oscillator had been used between the torch and the wrist that increased robot payload. In this paper, weaving motion is added to the equations of electrode motion planning. A smooth sinusoidal curve (Eq. (8)) is preferred to other curves such as triangular, trapezoidal, etc., where A represents the amplitude and fr represents the frequency:

$$\delta = \frac{A}{2}\sin\left(2\pi.fr.t\right) \tag{8}$$

The last rotation in Fig. 5 is the rotation angle of the torch, w, around its Z-axis Torch. In some applications such as welding, cutting, gluing, machining, etc., the rotation of end effector tool around its axial axis is not important, and it is used as one degree of redundancy called functional redundancy. It may be considered constant, or it can be used to optimize the path for predefined criteria.

In order to map the Torch frame to the Seam frame, firstly a transform L in the direction of the Z-axis Seam is done. Then, rotation w about the Z-axis Seam, rotation v about the Y-axis Seam, and rotation u about the X-axis Seam take place, respectively. At the end, a shift δ in the direction of the Y-axis Seam must be performed:

$$\begin{aligned}
{}^{Seam}_{Torch}T &= Tran_{y,\delta} \times \mathrm{Rot}_{X,u} \times Rot_{y,v} \times Rot_{z,\omega} \times \mathrm{Tran}_{z,l} \\
&= \begin{bmatrix} 1 & 0 & 0 & 0 \\ 0 & 1 & 0 & \delta \\ 0 & 0 & 1 & 0 \\ 0 & 0 & 0 & 1 \end{bmatrix} \begin{bmatrix} 1 & 0 & 0 & 0 \\ 0 & cu & -su & 0 \\ 0 & su & cu & 0 \\ 0 & 0 & 0 & 1 \end{bmatrix} \begin{bmatrix} cv & 0 & -sv & 0 \\ 0 & 1 & 0 & 0 \\ sv & 0 & cv & 0 \\ 0 & 0 & 0 & 1 \end{bmatrix} \begin{bmatrix} c\omega & -s\omega & 0 & 0 \\ s\omega & c\omega & 0 & 0 \\ 0 & 0 & 1 & 0 \\ 0 & 0 & 0 & 1 \end{bmatrix} \begin{bmatrix} 1 & 0 & 0 & 0 \\ 0 & 1 & 0 & 0 \\ 0 & 0 & 1 & l \\ 0 & 0 & 0 & 1 \end{bmatrix} \\
&= \begin{bmatrix} Cv\,C\omega + Su\,Sv\,S\omega & -Cu\,S\omega & Cv\,Su\,S\omega - C\omega\,Sv & -l\ (Sv\,C\omega - Cv\,Su\,S\omega) \\ Cv\,S\omega - C\omega\,Su\,Sv & Cu\,C\omega & -Sv\,S\omega - C\omega\,Su\,Cv & \mathrm{h} - l\ (Sv\,S\omega + Cv\,Su\,C\omega) \\ CuSv & Su & Cu\,Cv & l\,Cu\,Cv \\ 0 & 0 & 0 & 1 \end{bmatrix}
\end{aligned} \tag{9}$$

In the next section, the trajectory planning algorithm and the effect of robotic system redundancy, to improve the desired welding path, are discussed. In welding application, the planned path is irrelative to electrode rotation around its axial axis. It causes a functional redundancy of order one. The inherent redundancy due to the workpiece positioner and movable robot base is from the second order. So, generally, we have three degrees of kinematic redundancy.

3. Trajectory Planning Algorithm

In the previous section, the kinematic solution algorithm of intersecting pipes in the presence of motion redundancies was introduced. The path in joint space is generated by the algorithm shown in Fig. 6. This algorithm is surveyed in this section.

At the first step, the welding torch pose vector X, including the position and orientation of the electrode, is calculated. At the second step, the joint angles corresponding to the starting path node X(1) are calculated using analytical inverse kinematics. To have a smooth motion at the beginning and end of the path, at the third step, the acceleration and deceleration coefficients are defined (Fig. 7). The velocity at path nodes is determined. Then, the traveling time between two nodes is calculated. This time is irrelative to the weaving motion. Therefore, the distance between two nodes ΔS must be calculated regardless of the weaving motion. That is why at the first step the weaving motion was not taken into account and its related value $\delta = 0$ was used. At the fourth step, when a weaving path is needed, the HT ${}^{Seam}_{Torch}T$ in Eq. (1) must be modified by adding weaving amplitude using Eqs. (8) and (9). At the fifth step the time derivative of path $\dot{\mathrm{X}}$ is derived. Thus, from the first to fifth steps, the specifications of the desired path are calculated.

At the sixth step, the joint velocity $\dot{\mathrm{q}}$ is computed using the Jacobian-based method, $\dot{\mathrm{q}} = \mathrm{J}^{\#}\dot{\mathrm{X}}$, to which we will turn to in Section 4.1. At the seventh step, the joint angles are computed using numerical integration from joint velocity $\dot{\mathrm{q}}$.

https://doi.org/10.1017/S0263574718001418 Published online by Cambridge University Press

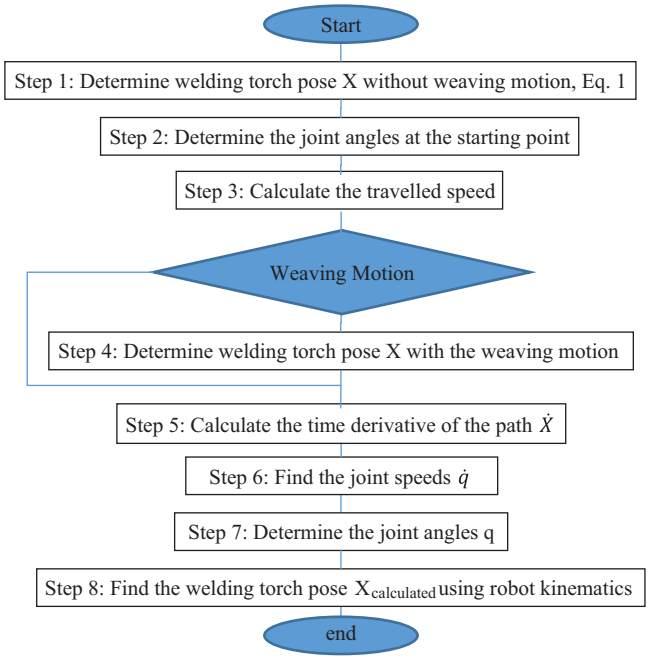

Fig. 6. Path planning algorithm.

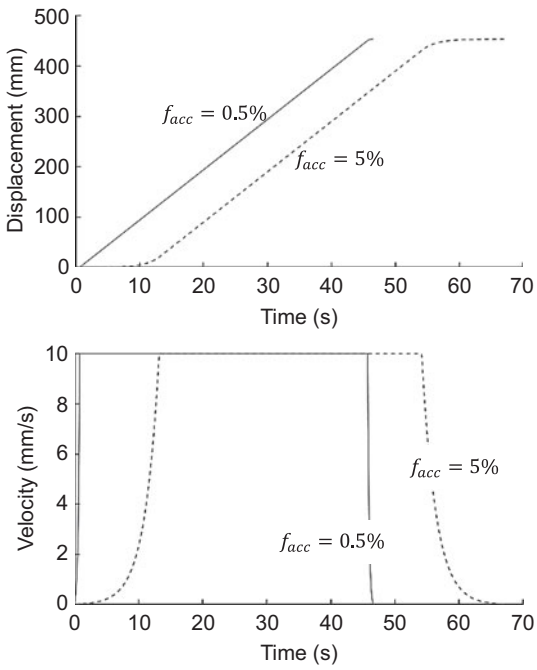

Fig. 7. Smooth movement between the start and end of the path by applying acceleration coefficient.

4. Simulation Studies Considering Kinematic Redundancy

In this research, a common industrial manipulator with 6 DOF is considered for the welding task. These robots have 6 DOF, 3 for position and 3 for orientation determination of the end effector. On the other hand, the rotation of welding electrode around its axis in the welding application is not important. Therefore, the use of an industrial robot with 6 DOF causes a degree of redundancy, called functional redundancy.

In addition, due to the pipe longitudinal dimension, some sections of the welding region may exceed from the robot's working space. Therefore, to reach the entire pipe's longitudinal sections,

https://doi.org/10.1017/S0263574718001418 Published online by Cambridge University Press

Table I. DH parameters (Romat 320), joint angles, and joint speed limits.

i	α_i	a_i	d_i	θ_i	**Joint angle limits**	**Joint speed limits**
0	90	0	d_0	−90	$-0.5\text{ m} < d_0 < +0.5\text{ m}$	500 mm/s
1	−90	250	0	θ_1	$-170° < \theta_1 < +170°$ [1]	151°/s
2	0	630	0	θ_2	$-180° < \theta_2 < +35°$	151°/s
3	−90	196	0	θ_3	$-210° < \theta_3 < +60°$	176°/s
4	90	0	720	θ_4	$-179° < \theta_4 < +179°$	290°/s
5	−90	0	0	θ_5	$-135° < \theta_5 < +135°$	338°/s
6	145	0	273	θ_6	$-300° < \theta_6 < +300°$	410°/s

[1] $-80° < \theta_1 < +260°$ (if robot base redundancy exists).

Table II. Geometrical and operational parameters.

Pipe geometry parameters, Fig. 3	$R = 220\text{ mm},\ r = 114\text{ mm},\ e = 0,\ \alpha = 90°$
Welding torch parameters, Fig. 5	$v = 0°,\ u = 51°,\ w = 35°,\ l = 0,\ \delta = 10\text{ mm}$
Weaving motion parameters	$D = 10\text{ mm},\ fr = 1\text{Hz}$
Welding speed	$V = 10\text{ mm/s}$

the base of the robot is placed on the roof or floor rail to reach the longitudinal direction of the pipe, resulting in system redundancy increase.

In pipe welding with large sizes, it is common to use a main pipe rotational positioner. Therefore, we studied the application with different redundancy conditions. In the first case, it is assumed that both manipulator base and main pipe are fixed, and the path is planned only with manipulator joint motion. In the second case, only the robot base is free to move while the main pipe is fixed, and in the third case, the main pipe is free to rotate together with base linear movement of the manipulator.

A common robotic cell is considered, while the results can be generalized for other robots installed whether on roof or floor rail. Figure 1 shows a robotic cell consisting of an industrial robot, installed on a roof rail. The joint angles and speed limits of this robot are stated in Table I, while the geometrical parameters of the main and branch pipes as well as the operational parameters of welding are stated in Table II.

4.1. Path planning only with manipulator

Here, two motion redundancies, including main pipe positioner and robot base motions, are ignored, so that the 6 DOF base manipulator ($n = 6$) and main pipe are fixed. Because arc welding is a 5 DOF task ($m = 5$), conducting arc welding with an industrial 6 DOF robot renders the robot functionally redundant. To resolve functional redundancy, we use a Jacobian-based method, $\dot{q} = J^{\#}\dot{X}$, where $\dot{q}$ is a $n \times 1$ vector, including joint speeds. The term $J^{\#}$ is pseudo-inverse of Jacobian and is a $n \times m$ matrix, defined as $J^{\#} = J^T \left(J\ J^T\right)^{-1}$. The pseudo-inverse joint velocity minimizes the norm among all joint velocities that minimize the task error norm.

In Fig. 8 the welding torch 3D space profile is shown, including position and orientation of the electrode. The simulation of robotic movement along this path between $180° \leq \theta \leq 360°$ is shown in Fig. 8, too. The robot base movement and weaving motion were neglected. The motion angle is 0, while the work angle is $u = 51°$. The electrode extension is $\delta = 10\text{ mm}$.

A uniform electrode advance along the welding path guarantees weld quality. As shown in Fig. 7, deceleration coefficient is equal to acceleration coefficient. It is seen that the total traveling time depends on the amount of acceleration coefficient, which is assumed to be f_{acc}= 0.5% or 5%. The components of welding torch position and velocity are shown in Fig. 9. Welding velocity is the sum of tree elements of torch velocity. A desired welding velocity profile is selected by the user. Welding velocity at the beginning and end of the path is less than its nominal value. It is useful because at path beginning it causes warming up of the welding electrode, while at path end it prevents end crater welding defect.

The path specifications in joint space, that is, joint angle q and joint velocity $\dot{q}$, are derived using inverse kinematics solution. It can be seen in Fig. 10 that joint q_1 at $325° \leq \theta_{Branch} \leq 360°$ exceeded its lower limit $q_{2min} = -170°$, as stated in Table I.

https://doi.org/10.1017/S0263574718001418 Published online by Cambridge University Press

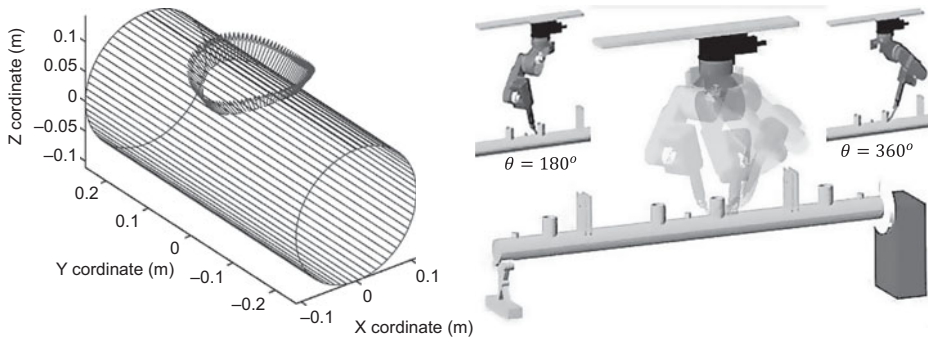

Fig. 8. Welding torch pose and robotic simulation in its desired path.

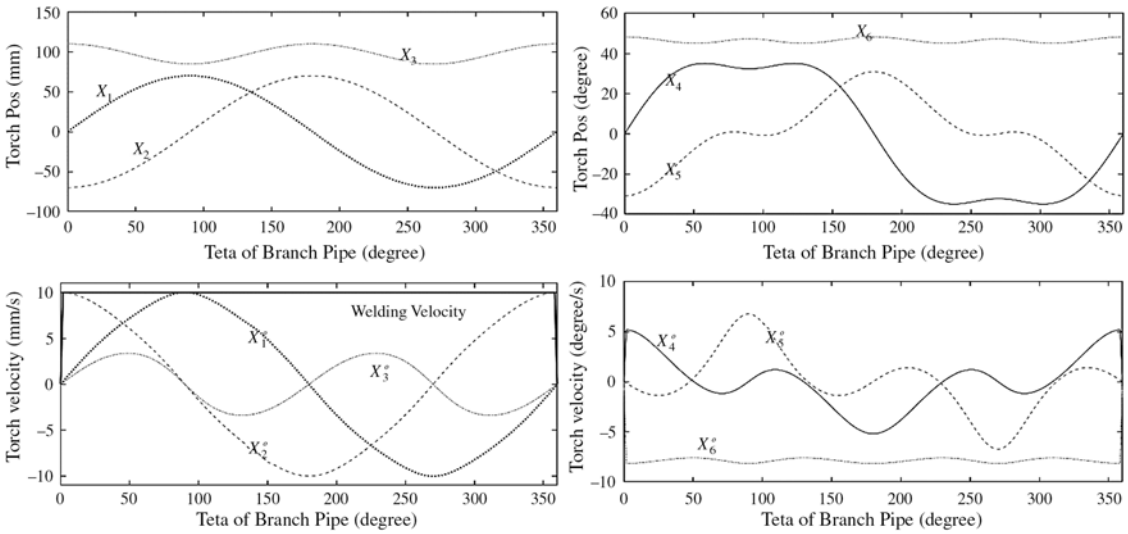

Fig. 9. History of variation of electrode position and velocity.

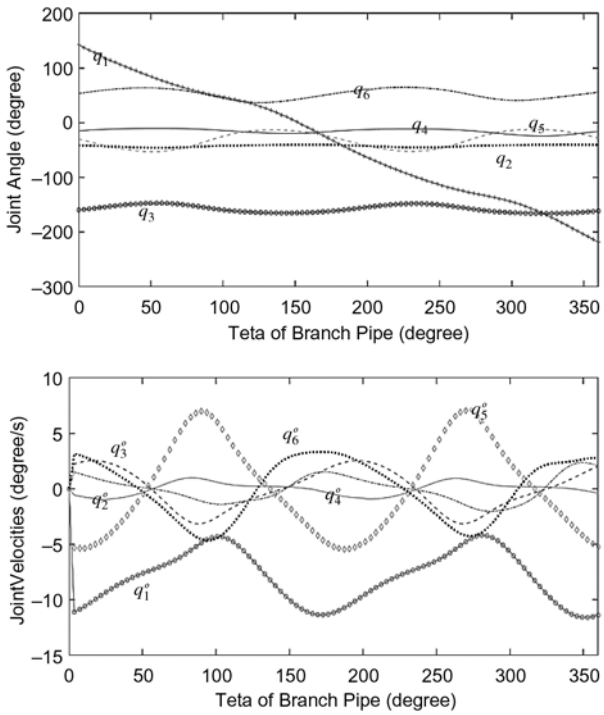

Fig. 10. History of joint angle and velocity variations.

https://doi.org/10.1017/S0263574718001418 Published online by Cambridge University Press

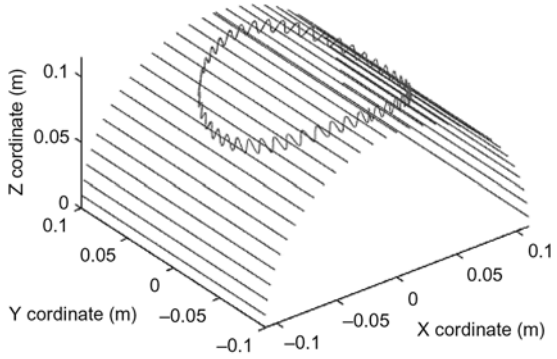

Fig. 11. Weaving motion included in path planning.

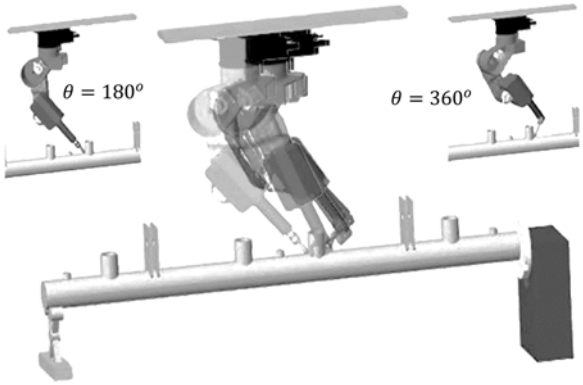

Fig. 12. The robot's motion simulation of planned path with base movement.

If a weaving path is desired, a planned path can be determined in the fourth step of the algorithm. It is shown in Fig. 11. The weaving motion is a sinusoidal curve with amplitude and frequency of 10 mm and 1 Hz, respectively.

4.2. Path planning with movable base

In our previous simulation study described in Section 4.1, a general solution without robot base and workpiece positioner was used for path planning. As discussed, one of the joints at some part of the path exceeded its admissible limits. It means that the robot following the desired weld path is impossible.

The redundancy that is used here is robot base movement. The robot's motion simulation by taking into account robot base movement is shown in Fig. 12. The welding torch 3D space profile is the same as the one described previously, Fig. 8.

The related joint angles and velocities are shown in Fig. 13. In this figure, q_0 in mm and $\dot{q}_0$ in mm/s shows the base movement and base velocity during welding. Other joints are robotic arm joints having the dimensions of degree and degree/s. With respect to the joint limits in Table I, the first joint in some part of the path, $164.8° \leq \theta \leq 202.2°$, exceeded its upper limit, and the fifth joint in some other part of the path, $319.5° \leq \theta \leq 360°$, exceeded its lower limit. Also, in the velocity graph, there is a jump in joint speed at $\theta = 159°$ that must be eliminated. For briefing just $\dot{q}_0$ and $\dot{q}_4$ are shown.

4.3. Redundancy resolution with task augmentation

Here, in order to produce a smooth path, the robot base redundancy and functional redundancy are employed for joint limit and singularity avoidance, while the redundancy of the main pipe positioner is used for making the welding position close to flat position, which is effective in improving weld quality.

https://doi.org/10.1017/S0263574718001418 Published online by Cambridge University Press

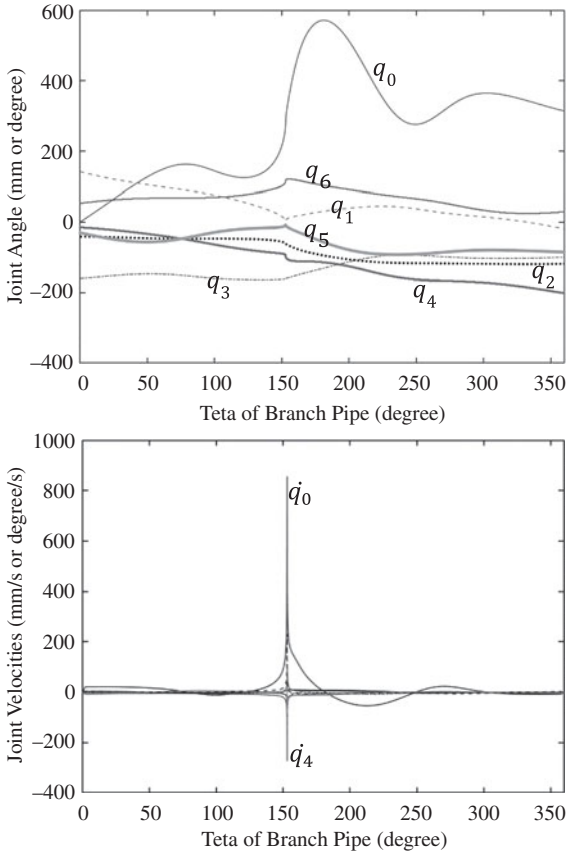

Fig. 13. Joint angles and velocities considering robot base redundancy.

Based on the latest rotational transformation in Fig. 5, the rotation angle of electrode w around its Z-axis is not interesting for welding applications. Now we define this coefficient empirically with a kinematic constraint as follows:

$$w = 35^\circ - \theta, \text{ and } \dot{w} = -\dot{\theta} \tag{10}$$

To better control the molten weld pool, the flat position is more effective than other welding positions, such as vertical, overhead, etc. The main pipe positioner is controlled to have flat welding conditions. For this purpose, a kinematic constraint is applied to the main pipe rotating angle β, such that the tip of the electrode remained at the highest point on the main pipe. From an observer's view of the Station frame during robotic motion, the end effector has no motion in the X direction, while in the Z direction it remained at a point equal to the radius of the main pipe. Consequently the position of the electrode during path traveling is $(0,\ y_{port},\ R)$. By embedding this position constraint in Eqs. (1) and (4), the rotation angle of the main pipe positioner β in terms of θ is obtained as:

$$\beta(\theta) = \arctan\left(-\frac{r\sin\theta + e}{\sqrt{R^2 - (r\sin\theta + e)^2}}\right), \text{ and } \dot{\beta} = f(\dot{\theta}) \tag{11}$$

The robotic motion simulation is shown in Fig. 14. The welding torch position components as well as main pipe rotation angle are shown on the left side of Fig. 14. Because the position components in directions X and X are constant, their related velocities in these directions are 0, and the velocity in direction Y is equal to the welding speed.

The joint angles in the presence of robot base, main pipe positioner, and functional redundancy are shown in Fig. 15. No joints exceeded its limits, as well as the path is smooth without any interruption.

https://doi.org/10.1017/S0263574718001418 Published online by Cambridge University Press

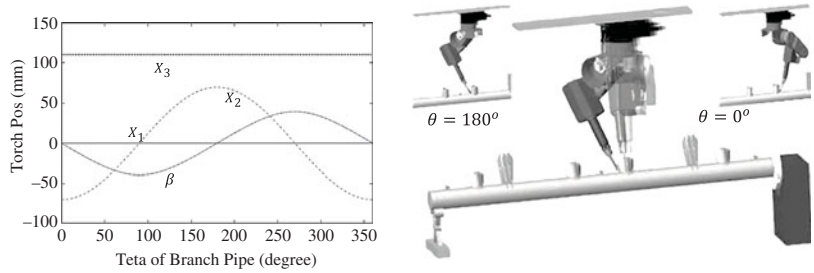

Fig. 14. Robotic motion simulation with workpiece positioned.

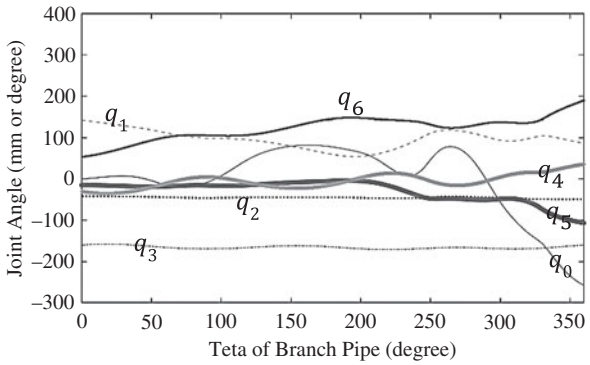

Fig. 15. Joint angles of the robot using all three redundancies.

5. Conclusion

A method to use kinematic and functional redundancies of the robotic system is proposed to avoid joint limits and singular conditions in the welding of complex pipe joints. To demonstrate the effectiveness of the proposed method, a 6 DOF industrial robot with mobile base and rotating system for the main pipe is used. At first, path planning was done with a fixed base manipulator with one excess functional redundancy in the sixth joint. In this case study, the fifth joint in some ranges of its motion exceeds its allowable limit. Then during the second simulation, the robot base linear motion is added as kinematic redundancy to the robotic motion. The final motion is smoother than the previous simulation case. But some joint limits are again violated during the motion, as well as some singular points exist during the motion. Finally, some additional task is augmented for electrode spatial configuration as well as a kinematic constraint for main pipe rotation, that is, extra kinematic redundancy. The Main pipe redundancy is used to bring the welding condition closer to the flat weld to improve weld quality. A smooth path without interruption and exceeding the joint limits is generated. To conclude, the use of additional DOF in redundant robotic systems can be effective in performing complex weld operations.

References

1. A. G. Ruiz, J. C. Santos, J. Croes, W. Desmet and M. M. da Silva, "On redundancy resolution and energy consumption of kinematically redundant planar parallel manipulators," *Robotica* **36**(6), 809–821 (2018).
2. D. Guo, K. Li and B. Liao, "Bi-criteria minimization with MWVN-INAM type for motion planning and control of redundant robot manipulators," *Robotica* **36**(5), 655–675 (2018).
3. S. Hwang, H. Kim, Y. Choi, K. Shin and C Han, "Design optimization method for 7 DOF robot manipulator using performance indices," *Int. J. Precis. Eng. Manuf.* **18**(3), 293–299 (2017).
4. Y. Huang and M. Fei, "Motion planning of robot manipulator based on improved NSGA-II," *Int. J. Control, Autom. Syst.* **16**(4), 1878–1886 (2018).
5. V. S. Chembuly and H. K. Voruganti, "Trajectory planning of redundant manipulators moving along constrained path and avoiding obstacles," *Procedia Comput. Sci.* **133**, 627–634 (2018).
6. J. Léger and J. Angeles, "Off-line programming of six-axis robots for optimum five-dimensional tasks," *Mech. Mach. Theory* **100**, 155–169 (2016).
7. A. Meghdari, D. Naderi and S. Eslami, "Optimal stability of a redundant mobile manipulator via genetic algorithm," *Robotica* **24**(6), 739–743 (2006).

https://doi.org/10.1017/S0263574718001418 Published online by Cambridge University Press

8. A. Atawnih, D. Papageorgiou and Z. Doulgeri, "Kinematic control of redundant robots with guaranteed joint limit avoidance," *Robot. Auton. Syst.* **79**, 122–131 (2016).
9. M. H. Korayem and H. Ghariblu, "Maximum allowable load on wheeled mobile manipulators imposing redundancy constraints," *Robot. Auton. Syst.* **44**(2), 151–159 (2003).
10. Y. Lu, X. Tian and J. Liang, "Track control in automated welding of saddle curve," *J. Sci. Ind. Res.* **69**(11), 811–817 (2010).
11. C. Chen, S. Hu, D. He and J. Shen, "An approach to the path planning of tube–sphere intersection welds with the robot dedicated to J-groove joints," *Robot. Comput.-Integr. Manuf.* **29**(4), 41–48 (2013).
12. Y. Liu, J. Zhao, Z. Lu and S. Chen, "Pose planning for the end-effector of robot in the welding of intersecting pipes," *Chin. J. Mech. Eng.-English Ed.* **24**(2), 264 (2011).
13. L. Wu, K. Cui and S.-B. Chen, "Redundancy coordination of multiple robotic devices for welding through genetic algorithm," *Robotica* **18**(6), 669–676 (2000).
14. F. Ren, S. J. Chen, S. Y. Yin and X. Y. Guan, "Modeling on weld position and welding torch pose in welding of intersected pipes," *Trans. China Weld. Ins.* **29**(11), 33–36 (2008).
15. T. Yao, Y. Gai and H. Liu, "Development of a robot system for pipe welding," **In**: *2010 International Conference on Measuring Technology and Mechatronics Automation*, Changsha, China (IEEE, 2010 March).
16. X. C. Tian and Y. Lü, "Trajectory control in automated welding of tubular joints," **In** *Applied Mechanics and Materials* (Z. Du and B. Liu, eds.) (Trans Tech Publ, Switzerland, 2010).
17. N. C. N. Doan and W. Lin, "Optimal robot placement with consideration of redundancy problem for wrist-partitioned 6R articulated robots," *Robot. Comput.-Integr. Manuf.* **48**, 233–242 (2017).
18. L. Shi and X. Tian, "Automation of main pipe-rotating welding scheme for intersecting pipes," *Int. J. Adv. Manuf. Technol.* **77**(5–8), 955–964 (2015).
19. L. Shi, X. Tian and C. Zhang, "Automatic programming for industrial robot to weld intersecting pipes," *Int. J. Adv. Manuf. Technol.* **81**(9–12), 2099–2107 (2015).
20. J. Li, L. Li, Z. Dong and D. Song, "An automatic posture planning software of arc robot based on SolidWorks API," *Mod. Appl. Sci.* **3**(7), 121 (2009).
21. L. Huo and L. Baron, "The self-adaptation of weights for joint-limits and singularity avoidances of functionally redundant robotic-task," *Robot. Comput.-Integr. Manuf.* **27**(2), 367–376 (2011).
22. F. Fahimi, *Autonomous Robots: Modeling, Path Planning, and Control* (Springer Science & Business Media, Berlin/Heidelberg, Germany, 2008), Vol. 107.

https://doi.org/10.1017/S0263574718001418 Published online by Cambridge University Press